Available online at www.sciencedirect.com
SCIENCE DIRECT
Polymer 46 (2005) 9243–9256
polymer
www.elsevier.com/locate/polymer

Structure-property relations of poly(propylene oxide) block copolymers with monodisperse and polydisperse crystallisable segments

Martijn van der Schuur[1], Jan de Boer[2], Reinoud J. Gaymans*

University of Twente, P.O. Box 217, 7500 AE Enschede, The Netherlands

Received 8 March 2005; received in revised form 6 July 2005; accepted 12 July 2005
Available online 10 August 2005

Abstract

Segmented block copolymers with poly(propylene oxide) and crystallisable segments were synthesized and their structure-property relations studied. As crystallisable segments, amide units based on poly(*p*-xylylene terephthalamide), were used. The length of the amide segment was varied and these segments either had a monodisperse or random length distribution (polydisperse). The poly(propylene oxide) used was end capped with 20 wt% ethylene oxide (EO-tipped) and had a molecular weight of 2300 g/mol (M_n, incl. EO-tips). These segmented block copolymers are model block copolymers to gain insight in the structure-properties behaviour of related semi-crystalline segmented block copolymers, like polyether(urethane–urea)s. The morphology of the polyether(ester–amide)s (PEEA) was studied with TEM, the thermal properties with DSC and DMTA and the crystalline structures with WAXD. The elastic behaviour of the block copolymers was investigated in tensile and compression.

Phase separation in PEEA's with crystallisable, short and monodisperse amide segments occurred by crystallisation, while with crystallisable random amide segments phase separation occurred through liquid–liquid demixing in combination with crystallisation. With short monodisperse amide segments, morphology of dispersed ribbons with a high aspect ratio was observed. PEEA's containing these monodisperse amide segments had higher moduli and better elastic properties as compared to PEEA's with random length amide segments. Increasing the length of the monodisperse amide segment increased the modulus and decreased the compression set of the corresponding blockcopolymers.

Keywords: Polyether(ester–amide); Morphology; Polyether(urethane–urea)

1. Introduction

Segmented polyurethanes, like polyether(urethane)s or polyether(urethane–urea)s (PEUU), are probably the most widely studied semi-crystalline segmented block copolymers and are mainly applied as fibers, coatings and foams. These materials consist of alternating mobile polyether segments with a low T_g and rigid urethane (or urea) segments with a high T_g and/or high T_m [1]. Above a critical length of either segment, this binary block copolymer system is thermodynamically unstable and phase separation occurs by liquid–liquid demixing [2,3]. Phase separation by liquid–liquid demixing is a relative slow process compared to crystallisation and may occur even in the melt, which is also known as melt phasing [13]. This liquid–liquid demixing is often followed by partial crystallisation of the rigid segments [2–9]. The resulting morphology of these block copolymers is, therefore, quite complex as it consists of more than two phases [4,5,10–12].

Segmented block copolymers have generally rigid segments with a random length distribution. These segments are referred to as random segments. The effect of rigid segment length distribution has been studied on segmented polyurethanes [14–17]. Block copolymers with monodisperse urethane segments, i.e. with a monodisperse length, were found to have higher softening temperatures, enhanced and less temperature dependent rubber moduli, higher tensile strengths and strains. The morphology of block copolymers with monodisperse rigid segments consisted of

* Corresponding author.
E-mail address: r.j.gaymans@utwente.nl (R.J. Gaymans).
[1] Present address: Océ-Technologies B.V., 5900 MA Venlo, The Netherlands.
[2] Present address: Pipelife Nederland B.V., 1600 AJ Enkhuizen, The Netherlands.

0032-3861/$ - see front matter © 2005 Elsevier Ltd. All rights reserved.
doi:10.1016/j.polymer.2005.07.041

long crystallites of polyurea segments embedded in a soft polyether phase [17,18]. The length of these crystallites was over 500 nm and the estimated thickness was 10 nm.

Segmented polyurethanes are thermally unstable, which complicates studies on their structure-property relations. Segmented polyamides, on the other hand, are thermally more stable, while having similar hydrogen bonding as the segmented polyurethanes. These block copolymers are, therefore, interesting model block copolymers to mimic the structure-property relations of semi-crystalline segmented PEUU's. The morphology of segmented polyether(ester–amide)s (PEEA) with short monodisperse amide segments also consists of uniform thin crystalline ribbons with high aspect ratios [19,20]. These ribbons are randomly dispersed in the amorphous matrix. Short monodisperse diamide segments based on 1.5 repeat unit of poly(*p*-phenylene terephthalamides) or tetra-amide segments based on 2.5 repeating unit nylon-6,T and poly(tetramethylene oxide) (PTMO) were used. These segments were found to have a high degree of crystallisation and the copolymers have a relatively high and temperature independent modulus in the rubbery region. The use of the monodisperse tetra-amide segments also provided high elasticity of the corresponding block copolymer in spite of the relatively higher modulus obtained, which makes these segmented block copolymers interesting materials for TPE applications.

The research described in this paper focuses on the structure-property relations of poly(propylene oxide) based PEEA copolymers with crystallisable amide segments (Fig. 1). The rigid amide segments of these segmented block copolymers resemble the structure of the rigid segments in PEUU's.

It is, therefore, expected that the results of this study also give insight in the structure-property relations of PEUU's. The rigid amide segment of the PEEA's studied is based on poly(*p*-xylylene terephthalamide), which is a semi-crystalline polymer having a glass transition of 225 °C and a melting temperature >300 °C [21]. The mobile segment used is poly(propylene oxide) end capped with ethylene oxide groups to increase the reactivity (PEO–PPO–PEO).

The possible morphologies of the amide segments are proposed in Fig. 2. With short amide segments no liquid–liquid demixing (melt phasing) takes place, and at high temperatures the melt is homogenous (phase A) (Fig. 2(a)) [22]. On cooling from the homogenous melt the amide segments crystallise (phase B) and form crystalline ribbons in the soft matrix (Fig. 2(b)). With long amide segments ($x \geq 3$) (partially) liquid–liquid demixing takes place (phase C) in the melt and spherical amide domains are formed (Fig. 2(c)). On cooling this liquid–liquid demixed material, crystallisation of the amide segments may occur in the continuous (phase B) (Fig. 2(d)). As the liquid–liquid demixed phases are small crystallisation in these phases is probably not taking place. Segmented PEEA's that do not crystallise are known to have relative low moduli and poor elastic properties [22].

It is interesting to study the influence of the result of crystallisation and liquid–liquid demixing, on the tensile and elastic properties of segmented copolymers with crystallisable segments. In these segmented block copolymers liquid–liquid demixing can only be avoided if long segments are completely absent [22]. This can be accomplished by using short monodisperse amide segments. Also interesting is to examine the effect of the thickness of the crystallites on the tensile and elastic properties. Segmented copolymers were, therefore, synthesized with having either crystallisable monodisperse or random amide segments. In addition, the length of the monodisperse amide segments (x_m) and the random amide segments (x_r) were varied.

2. Experimental

2.1. Materials

Dimethyl terephthalate (DMT), terephthaloyl dichloride, phenol, *p*-xylylene diamine, tetra-isopropyl orthotitanate (Ti(i-$OC_3H_7)_4$), *m*-xylene, toluene, *N*-methyl-2-pyrrolidone (NMP), osmium tetroxide (OsO_4) (4 wt% solution in water), and formaldehyde (37 wt% solution in water) were purchased from Aldrich. Irganox 1330 was obtained from CIBA. These materials were used as received. Poly(propylene oxide)s end capped with 20 wt% ethylene oxide (EO) with a M_n of 2300 was a gift from Bayer AG (Acclaim Polyol PPO-2220 N). Diphenyl terephthalate (DPT) was synthesized as described before [23].

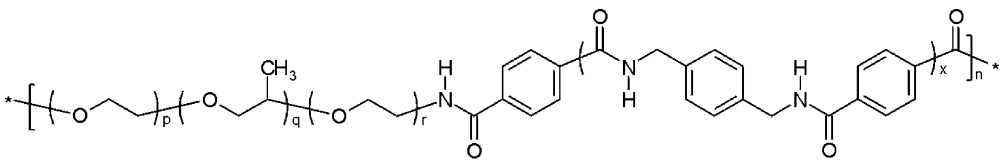

-[-EO-PPO-EO-T-(Xp-T)x-]n-

Fig. 1. The structure of a PEEA based on poly(propylene oxide) end capped with poly(ethylene oxide) and crystallisable segments based on poly(*p*-xylylene terephthalamide). The amide segment length is denoted as *x*.

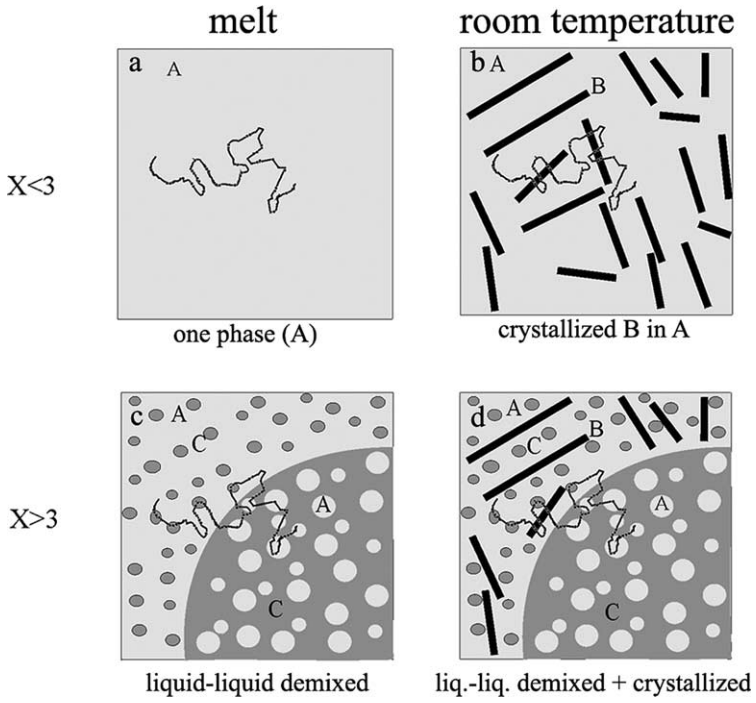

Fig. 2. Schematic representation of the expected morphologies depending on amide segment length (x) of the PEEA in the molten state and at room temperature. A, amorphous soft matrix (+dissolved amide segments); B, crystallised short amide segments; C, liquid–liquid demixed amide segments.

2.2. Synthesis of monodisperse bisester–oligoamide precursors with amide segment length x

The synthesis of monodisperse bisester–oligoamide precursors has been described before [23]. TX_pT-diphenyl ($x_m=1$) was synthesized with a mono uniformity of 90 mol%, i.e. 90 mol% of the bisester–oligoamide segments has length $x=1$ (bisester–diamide). TX_pTX_pT-diphenyl ($x_m=2$) was synthesized with a uniformity of 96 mol%. The uniformity is defined as the mol fraction of segments of the desired length and a uniformity of 90% means that the M_w/M_n for those segments is less than 1.02 [23].

2.3. Synthesis of polyether(ester–amide)s with monodisperse amide segments

An example is given in the case of a polyether(ester–amide) with tetra-amide segments with length $x_m=2$. A 250 ml stainless steel vessel equipped with magnetic coupled stirrer (Autoclave, type cmd 075) was charged with PEO–PPO–PEO_{2300} (20.0 g, 8.69 mmol), TX_pTX_p T-diphenyl (7.39 g, 8.69 mmol), 100 ml NMP and 1 wt% Irganox 1330 (based on PPO) under nitrogen flow (the magnetic coupled stirring device was important to obtain high vacuum conditions). The reaction mixture was stirred under N_2-flow, heated to a temperature of 120 °C in 1 h, and maintained for 2 h at 120 °C. Hereafter, the temperature of the reaction mixture was slowly raised to 250 °C in 1 h. Catalyst (2.0 ml, 0.05 M $Ti(OC_3H_7)_4$ in *m*-xylene) was added to the reaction mixture when the temperature reached 150 °C. Thereafter, low vacuum (10–1 mbar) was applied for 1 h and finally high vacuum (0.1–0.08 mbar) for 2 h at 250 °C. Subsequently, the product was cooled to room temperature whilst maintaining the high vacuum. The polymers were dried in vacuum at 70 °C overnight before use.

2.4. Synthesis of polyether(ester–amide)s with random amide segments

An example of a polymerization is given in the case the random amide segments have an average length $x_r=3$. A stainless steel vessel equipped with magnetic coupling stirrer (Autoclave, type cmd 075) was charged with PEO–PPO–PEO_{2300} (20.0 g, 8.69 mmol), *m*-xylylene diamine (3.54 g, 26.0 mmol), DPT (11.1 g, 35.0 mmol), 100 ml NMP and 1 wt% Irganox 1330 (based on PPO) under a nitrogen flow. The reaction mixture was stirred under N_2-flow to a temperature of 120 °C and kept for 2 h at 120 °C. Hereafter, the temperature was increased in 1 h to 250 °C and maintained for 2 h. Catalyst (2.0 ml, 0.05 M $Ti(OC_3H_7)_4$ in *m*-xylene) was added to the reaction mixture when the temperature reached 150 °C. Thereafter, low vacuum (10–1 mbar) was applied for 1 h and finally high vacuum (0.1–0.08 mbar) for 2 h. Subsequently, the product was cooled to room temperature whilst maintaining the high vacuum. The polymers were dried in vacuum at 70 °C overnight before use.

2.5. Viscometry

Inherent viscosities of polymer samples were measured at a concentration of 0.1 g/dl in phenol/1,1,2,2-tetrachloroethane (1:1 molar mixture) at 25 °C using a capillary Ubbelohde 1B.

2.6. ^1H NMR

^{1}H NMR spectra of the block copolymers were recorded on a Bruker AC 300 spectrometer at 300.1 MHz. Deuterated trifluoro acetic acid (TFA-*d*) was used as the solvent. The amide segment length x was calculated from ^{1}H NMR spectra and is the ratio of the integral of the peaks at 8.0 and 8.1 ppm ($I_{b+b'}$) (terephthalic amide side) and the integral of the peak at 8.5 ppm (I_a) (terephthalic ester side) [22,23].

2.7. Transmission electron microscopy (TEM) [24]

A small drop (40 μl) of a 0.3 wt% solution of polymer in hexafluoro isopropanol (HFIP) was cast on a carbon coated copper grid (200 mesh). Subsequently, the grid with polymer film was heated at 20 °C/min to 20 °C above the flow temperature and kept at that temperature for 10 min using the DSC apparatus. After that, the material was allowed to cool at 3 °C/min to 40 °C below the melting temperature. Annealing at this temperature was conducted for 10 min after which the sample was allowed to cool to room temperature at 3 °C/min. This special heat treatment was necessary to erase any solvent effects generated during casting and to allow crystallisation, if any, in these ultra thin films ($\pm$50 nm). The treated samples were stained in 1 wt% osmium tetra-oxide/formaldehyde solution for 1 h at 40 °C. (The use of the formaldehyde solution provided a higher contrast as compared to OsO_4 vapour or solution staining). TEM measurements were performed with a Phillips CM30 at an accelerating voltage of 300 kV.

2.8. Injection moulding

Test specimens, bars of $70\times9\times2$ mm^3, were prepared by processing on an Arburg H manual injection moulding machine. In case of monodisperse amide segments, the barrel temperature was set to 50–60 °C above the flow temperature as measured by DMTA. However, with random amide segments the barrel was set to 100–150 °C above the flow temperature as measured by DMTA. Test bars prepared by injection moulding were stored at room temperature for about 2 weeks before measuring. All samples were dried in vacuum at 70 °C overnight before use.

2.9. Dynamical mechanical thermal analysis (DMTA)

The storage (G') and loss modulus (G'') as function of temperature were measured on injection moulded test bars ($70\times9\times2$ mm^3) using a Myrenne ATM3 torsion pendulum at a frequency of 1 Hz. The samples were first cooled to -100 °C and then subsequently heated at a rate of 1 °C/min and 0.1% strain. The glass transition temperature was determined as the maximum of the loss modulus. The flow or softening temperature (T_{flow}) was defined as the temperature where the storage modulus reached 1.0 MPa. The flex temperature (T_{flex}) is defined as the temperature at the start of the rubber plateau region, the intersection of the tangents.

2.10. DSC

DSC spectra were recorded on a Perkin–Elmer DSC7 apparatus, equipped with a PE7700 computer and TAS-7 software. The test samples (polymerisation powder) were dried in vacuum at 70 °C overnight. The sample (5–10 mg) was heated at a rate of 20 °C/min up 20 °C above their T_m, cooled to room temperature and heated again. The second heating scans were used to determine the melting temperature of the polymer. The melting temperature (T_m) was taken as the temperature of the maximum of the endotherm. The first cooling curve was used to determine the crystallisation temperature, which was taken as the onset of crystallisation. The undercooling ($\Delta T = T_m - T_c$) was calculated and is used as a measure of the rate of crystallisation.

2.11. Shore A hardness

The hardness of the PEEA's was measured after injection moulding using a Zwick HHP 2001 shore A meter (ISO R 868/DIN 53505). The shore A hardness of a sample was determined as the average of five measurements.

2.12. Compression set

The samples for compression set were cut from injection moulded bars. The compression set was measured according to the ASTM 395 B standard. After 24 h at room temperature the compression (25%) was released at room temperature. After half an hour, the thickness of the samples was measured. The compression set is defined as:

$$\mathrm{CS} = \frac{d_0 - d_2}{d_0 - d_1} \times 100\% \quad (1)$$

d_0, thickness before compression (mm); d_1, thickness after compression (mm) (here $d_1 = 1.65$ mm); d_2, thickness 30 min after release of compression (mm).

The calculated compression sets were taken as the average of three measurements. The compression set measured as function of time was done at room temperature.

2.13. WAXD

X-ray diffraction data of compression moulded 1 mm thick samples were collected with a Phillips PW3710

X'Pert-1 diffractometer in Bragg–Brentano geometry, using a θ compensating divergence slit (12.5 mm in length). The Cu $K_{\alpha 1}$ radiation of 1.54056 Å was obtained with a curved graphite mono-chromator. Collection of diffraction data was conducted at increasing temperatures in a nitrogen atmosphere, using a low background spinning (1 rev/s) specimen holder. The data were collected in a range of $2\theta = 4$–$60°$ at steps of 0.1° and 30 min per scan. The experiment started with a measurement at 25 °C after which the temperature was raised to 100 °C with 2 °C/min and further to 275 °C taking measurements after every 25 °C. Compression molded samples were prepared at 300 °C for 3 min and a pressure of 7.5 bar, after which the samples were cooled under pressure to room temperature with approximately 5 °C/min.

2.14. Cyclic tensile test

Cyclic stress–strain experiments were conducted on injection molded bars cut to dumbbells (ISO 37 type 3) to measure the tensile set of the block copolymer samples. A Zwick Z020 universal tensile machine equipped with a 500 N load cell was used to measure the stress as function of strain for each loading and unloading cycle at a strain rate of $3.33 \times 10^{-2}\ s^{-1}$ (test speed of 50 mm/min). The strain of each loading–unloading cycle was increased (stair-case loading) and the tensile set was determined as function of the applied strain. The tensile set was calculated from the following relation:

$$\text{Tensile set} = \frac{\Delta\varepsilon_{\text{remaining}}}{\Delta\varepsilon_{\text{cycle}}} = \frac{\varepsilon_{\text{r,cycle}(i)} - \varepsilon_{\text{r,cycle}(i-1)}}{\Delta\varepsilon_{\text{cycle}}} \times 100\% \quad (2)$$

With $\varepsilon_{\text{r,cycle}(i)}$ the remaining strain at the end of cycle i and with $\varepsilon_{\text{r,cycle}(i-1)}$ the remaining strain at the end of the preceding cycle $i-1$.

3. Results and discussion

Poly(propylene oxide) based segmented polyether(ester–amide)s (PEEA) with crystallisable amide segments were made and the influence of morphology on polymer properties were studied. Two PEEA series were evaluated, with amide segments with a monodisperse (x_m) and with a random amide segment length distribution (x_r). The poly(propylene oxide) used is end capped with 20 wt% ethylene oxide (PEO–PPO–PEO) and has a number average molecular weight of 2300 g/mol (PEO–PPO–PEO_{2300}). The properties of the copolymers are summarized in Table 1 and discussed in detail afterwards.

3.1. Synthesis of the polyether(ester–amide)s

The copolymers were synthesized by starting with solution in NMP and ending in the melt. The block copolymers with monodisperse amide segments have relatively high molecular weights (η_{inh} of 1.1–1.9 dl/g). However, the inherent viscosities of polymers with random amide segments decreases strongly with amide segment length (1.58–0.53 dl/g) (Table 1).

When amide segments of monodisperse length ($x_m = 1$ and $x_m = 2$) were used, the PEEA's obtained were transparent both in the melt at 280 °C and at room temperature. Therefore, it is assumed that melt phasing (liquid–liquid demixing) in PEEA's with monodisperse diamide ($x_m = 1$) and tetra-amide segments ($x_m = 2$) is absent. These results correspond to previous reported results on similar PPO-based block copolymers [22] and PTMO-based block copolymers [19,20]. The fact that these semi-crystalline block copolymers are transparent also at room temperature implies that the crystallites (Fig. 2(b)) are too small to scatter light [19,20,22].

During the melt synthesis at 250 °C of block copolymers having a random amide segment length distribution, melt phasing was observed. This is probably due to liquid–liquid demixing of the amide segments with lengths of 3 and higher ($x \geq 3$) (Fig. 2(c)). These longer segments are always present in a randomly distributed system [22]. The phase-separated domains are apparently sufficiently large to scatter light. This phase separation in the melt is accompanied by a lowering of the inherent viscosity [1,19] (Table 1). The phase separation in the melt, thus, hinders the synthesis of high molecular weight block copolymers. The inherent viscosity of $x_r = 2$ of 1.65 is unexpected high. These materials are also opaque at room temperature.

The average amide segment length x, calculated by ^1H NMR, was for the random length amide segments higher than expected, i.e. based on monomer feed compositions (Table 1). Some diphenyl terephthalate may have reacted with two PEO–PPO–PEO segments thereby extending the PEO–PPO–PEO and as a result of this is the amide segment length also increased without that the amide content is increased.

3.2. Morphology

The morphology of the PEEA's with monodisperse and random amide segments ($x = 2$) and PEO–PPO–PEO_{2300} was studied by means of transmission electron microscopy (TEM). The staining agent OsO_4-formaldehyde solution [24,25] provided high contrast. Lothmar et al. [24] used a solvent casting technique, to obtain ultra-thin sections (< 100 nm), followed by heating the film above the melting temperature to erase any solvent effects generated by solvent casting and subsequent slow cooling to allow crystallisation. No significant differences between the TEM

Table 1
Properties of PEEA's with crystallisable amide segments with monodisperse (x_m) or random (x_r) segment length and PEO–PPO–PEO_{2300}

	x[a]	x[b] (NMR)	$T(X_pT)_x$ (wt%)	Melt[c]	η_{inh} (dl/g)	T_g (°C)	T_{flex} (°C)	T_{flow} (°C)	G' 25 °C (MPa)	CS (%)
Monodisperse: x_m										
-TX_pT-	1	–	11.2	T	1.89	−60	−44	60	18	37
-TX_pTXpT-	2	–	19.2	T	1.14	−65	−53	215	22	11
Random: x_r										
-$T(X_pT)_1$-	1	1.01	11.7	O	1.58	−61.	−41	140	2.1	22
-$T(X_pT)_{1.5}$-	1.5	1.70	16.8	O	0.68	−60	−40	155	3.2	33
-$T(X_pT)_2$-	2	2.11	19.6	O	1.65	−61	−41	179	6.5	27
-$T(X_pT)_{2.5}$-	2.5	3.16	26.5	O	0.53	−59	−40	205	13	35
-$T(X_pT)_3$-	3	3.59	29.1	O	0.55	−59	−41	210	16	42

[a] Amide length from monomer feed.
[b] Amide length from NMR.
[c] Melt: T, transparent; O, opaque.

images of samples prepared by the solvent casting technique or by cryo ultra-microtomy were reported by the authors.

The TEM micrograph of the PEEA with monodisperse crystallisable tetra-amide segments ($x_m = 2$) reveals ribbons of ±2–5 μm in length and several nm thick (~5 nm) (Fig. 3(a) and (b)). The crystallites are randomly dispersed in an amorphous matrix and the crystalline ribbons have an aspect ratio of 400–1000. Large spherical domains were not observed. The morphology with crystalline ribbons is schematically presented in Fig. 2(b).

With random amide segments ($x_r = 2$) the morphology is more complex (Fig. 3(c) and (d)). Visible are large spherical domains and crystalline ribbons. The spherical domains are 1–2 μm in diameter, which is very large, compared to the amide segment length. The crystalline ribbons are about 400 nm long and 5–10 nm thick. In the light coloured regions also vaguely many small particles can be seen (Fig. 3(c)).

Phase separation in block copolymers with random amide segments occurs probably by liquid–liquid demixing in combination with crystallisation. Liquid–liquid demixing in PEEA's is induced if the amide segment length is $x \geq 3$ and results in a dispersion of spherical domains in a soft matrix [22]. The shorter amide segments ($x < 3$) are expected to phase separate only through crystallisation and form crystalline ribbons outside the liquid–liquid demixed domains. The spherical liquid–liquid demixed domains, observed for these PEEA's, are, however, too large to consist of only amide segments and must, therefore, contain a PEO–PPO–PEO phase as well (Fig. 2(d)) [22]. Whether the segregated amide segments in the liquid–liquid demixed domains have crystallised is yet not clear as nucleation in small particles is difficult. The aspect ratio of the crystallites with the random length distribution is 50–100, this is a factor ten lower than with the monodisperse length segments.

3.3. DSC

DSC spectra of the block copolymers with monodisperse tetra-amide segments show two melting endotherms and two crystallisation exotherms (Fig. 4 and Table 2). The two melting endotherms may be ascribed to different structures of the crystalline amide phase in the PEEA. This behavior is quite common for polyamides and the first transition is generally referred to as a Brill transition [26].

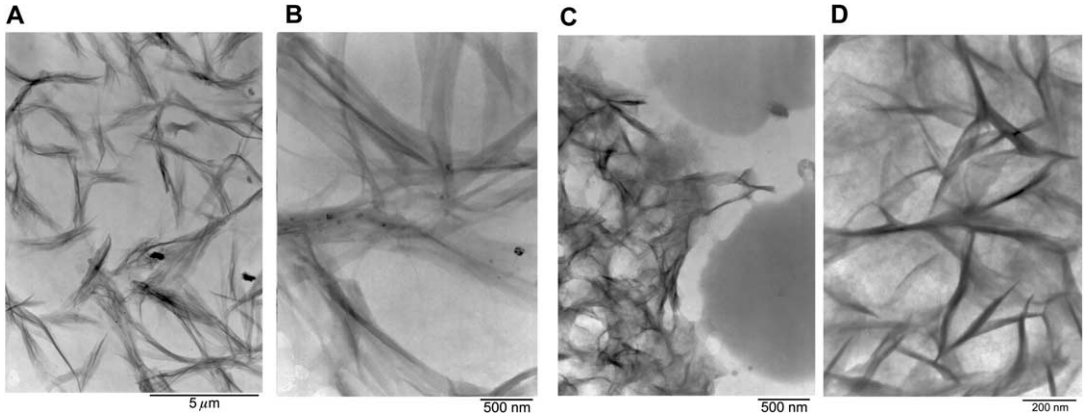

Fig. 3. TEM micrographs of PEO–PPO–PEO_{2300} based semi-crystalline PEEA's: A and B, monodisperse tetra-amide segments ($x_m = 2$, 19.2 wt% amide); C, random amide segments ($x_r = 2$, 19.6 wt%) and D, section of C in between spherical domains.

Two crystallisation exotherms have also been observed before in the DSC-spectra of PTMO-based PEEA's and also with PEO–PPO–PEO-based PEEA's with monodisperse tetra-amide segments based on nylon 6,T [20]. This behaviour is probably new to the use of monodisperse crystallisable tetra-amide segments and has not been observed on copolymers having monodisperse diamide segments [20]. The melting temperature for $x_m=1$ is 63 °C and for $x_m=2$ is 209 °C and which are close to the flow temperatures as measured by DMTA (Table 1). This increase in the melting temperature with increasing amide segment length (x) can be explained by the increase in crystal thickness, as described by Hoffman [27] and by an increase in the crystallinity (higher amide content) as described by Flory [28].

The enthalphies of melting were low due to the low amide contents and often difficult to determine well. The best measurable enthalpies were for x_m and x_r two and their values were, respectively, 14 and 1.1 J/g. An undercooling ($\Delta T=T_m-T_c$) of only ± 5 °C was found for PEEA's having monodisperse tetra-amide segments.

With random amide segments the melting temperature increases by increasing the average amide segment length x_r (Table 2). Block copolymers with the longer amides segments have undercooling values that are still remarkable low (11 °C). This suggests that also the longer random length segments crystallise very fast. Possibly some extra long segments act as a nucleation site for the crystallisation of other segments.

3.4. Hardening rate (shore A hardness)

Slow crystallisation processes of segmented block copolymers can be followed by measuring the hardening rate, i.e. the hardness of the material as function of time just after melt processing [1]. The hardness, here measured in shore A, is proportional to the logarithm of the modulus, which in turn is related to the crystallinity. As the crystallinity of a block copolymer increases, the modulus and hardness increase accordingly. In Fig. 5 the hardening rate, i.e. the increase in shore A hardness of the PEEA's with time, measured at room temperature, is presented.

With monodisperse diamide segments ($x_m=1$) the hardness of the corresponding block copolymers is initially very low, however, after 2500 s the hardness starts to increases. The increase in hardness is due to crystallisation of the monodisperse diamide segments. The slow increase is probably due to the low melting temperature of this diamide copolymer (60 °C) and, thus, the small window of crystallisation. The final hardness for block copolymers with $x_m=1$ is higher than the hardness of the block copolymers with random amide segments ($x_r=1$ and 2), but lower than for polymer with monodisperse tetra-amide segments ($x_m=2$). This is in line with the trends observed for the storage modulus as measured by DMTA (Table 1).

The hardness of the polymer with monodisperse tetra-amide segments ($x_m=2$) is obtained almost instantaneously at a maximum, 91 shore A. Crystallisation of monodisperse tetra-amide segments is, therefore, considered to be much faster than the crystallisation of monodisperse diamide segments. Also with random amide segments the hardness is very fast at a plateau value and increases somewhat with time. The hardness value for $x_r=1$ is low and is somewhat higher for $x_r=2$. The trend in these hardness values corresponds to the moduli in Table 1.

3.5. WAXD

The order of monodisperse crystallisable amide structures present in the block copolymers as a function of temperature (25–275 °C) was studied with wide-angle X-ray diffraction (WAXD).

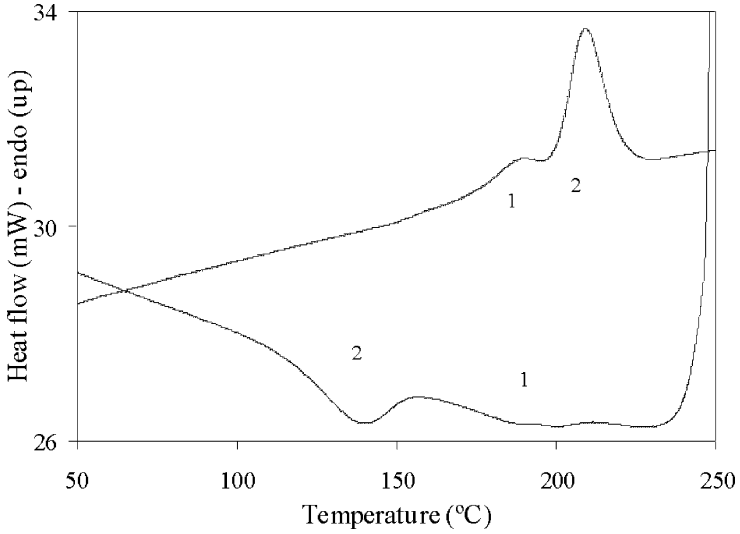

Fig. 4. DSC trace with monodisperse tetra-amide segments, second heating curve and first cooling curve are shown.

Table 2
Thermal properties (DMTA and DSC) with monodisperse and random crystallisable amide segments and PEO–PPO–PEO_{2300} segments

	X	$T(X_pT)_x$ (wt%)	T_{flow} (°C)	T_{m1} (°C)	T_{c2} (°C)	T_{m2} (°C)	T_{c1} (°C)	ΔT (°C)
Monodisperse: x_m								
$-TX_pT-$	1	11.2	60	–	–	63	–	–
$-TX_pTX_pT-$	2	19.2	215	188	138	209	204	5
Random: x_r								
$-T(X_pT)_1-$	1.01	11.7	140	–	–	–	–	–
$-T(X_pT)_{1.5}-$	1.70	16.8	155	–	–	171	–	–
$-T(X_pT)_2-$	2.11	19.6	179	–	–	178	–	–
$-T(X_pT)_{2.5}-$	3.16	26.5	205	–	–	186	175	11
$-T(X_pT)_3-$	3.59	29.1	210	–	–	194	183	11

X-ray diffractograms with monodisperse crystallisable amide segments ($x_m=2$) show broad peaks at 2θ-values of: 20 and 44°, and shoulders at 18 and 23° (Fig. 6).

The broad peak at 20° is from the amorphous PEO–PPO–PEO phase, which broadens and shifts to lower 2θ values (higher d-spacing) with increasing temperature. The remaining reflections are ascribed to the crystalline amide segments. The low scattering intensity of the amide crystallites can be due to the small thickness of the crystallites ($\pm$4 nm) [29] and the low concentration. The peaks at 18° ($d=4.9$ Å) and 23° ($d=3.6$ Å) both shift to lower 2θ values with increasing temperature and have disappeared at a temperature of 250 °C, which is 40 °C above the melting temperature. This suggests that in the melt of the PEEA's (at 200–250 °C) organized amide structures are still present, which has been ascribed before to liquid-crystalline behaviour. The broad peak at 44° is also related to reflections of the amide phase ($d=2.0$ Å) and shifts with temperature to higher values of 2θ without disappearing.

With random amide segments ($x_r=2$) on top of a broad deflection at 20° several sharp reflections are present at: 19.7, 21.1, 26.6, 28.3° and a small reflection at 18.6° (Fig. 7).

A second broad reflection is at 44°. The peaks at 2θ-values of 19.7° ($d=4.5$ Å), 21.1° ($d=4.2$ Å), 26.6° ($d=3.4$ Å) and 28.3° ($d=3.2$ Å) are associated with reflections of the crystalline amide phase.

All diffraction peaks shift to slightly higher values of 2θ with temperature without disappearing. This presumes the persistence of an ordered phase at temperatures above the melting temperature of the block copolymer, this possibly due to a small fraction of longer segments. The broad peaks at 20 and 44° are also observed in the block copolymers with monodisperse amide segments and are assigned to the amorphous PEO–PPO–PEO and amide phase, respectively. Obviously, with random amide segments sharper

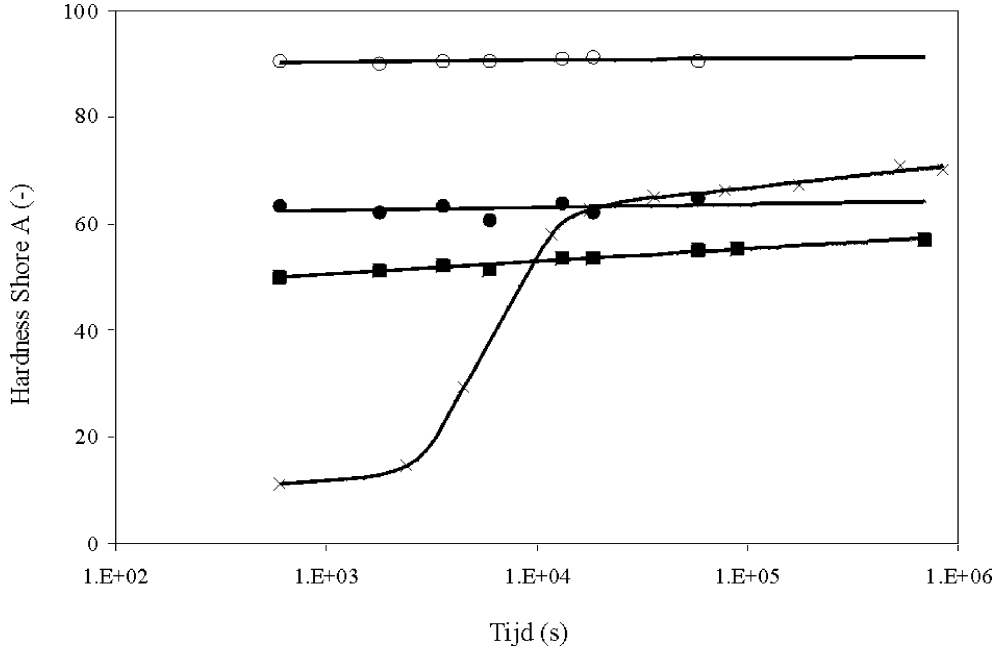

Fig. 5. Hardening rate: Shore A (at room temperature) of PEEA's with random and monodisperse amide segments as function of time after melt processing. Amide segment length x: (■) $x_r=1$; (●) $x_r=2$; (×) $x_m=1$; (○) $x_m=2$.

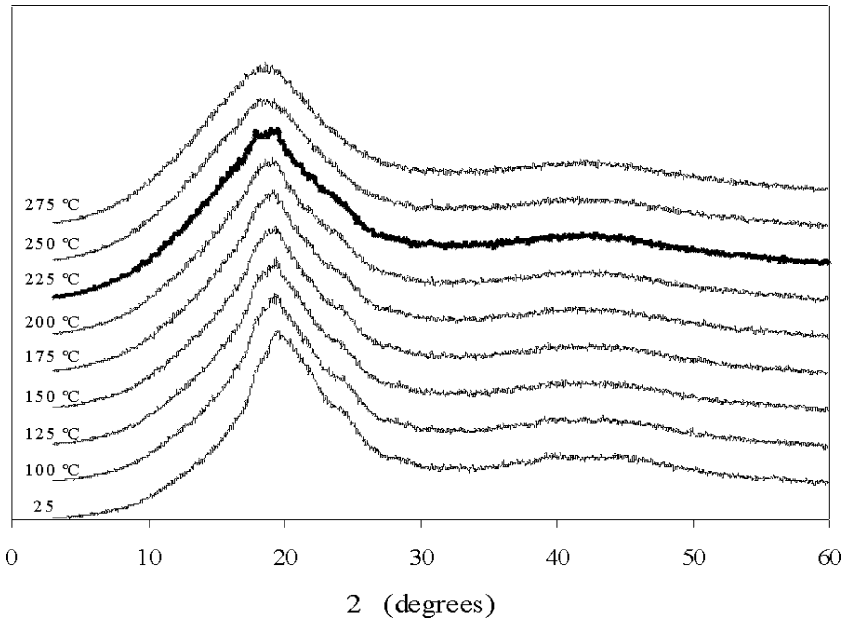

Fig. 6. WAXD patterns as function of temperature with monodisperse amide segments ($x_m=2$) ($T_{flow}=215$ °C).

'crystalline' reflections exist than with monodisperse amide segments. This may be due to the presence of thicker crystallites, which scatter stronger.

3.6. DMTA

PEEA's with monodisperse diamide or tetra-amide segments were studied by DMTA and the storage modulus and loss modulus as function of temperature were measured (Table 1, Fig. 8). The glass transitions for these copolymers are sharp and located at low temperatures (low T_g), the flex temperatures (T_{flex}) are low, the storage moduli at 25 °C are high considering the amide concentration and there is hardly any temperature dependence of the modulus in the plateau region. The flow temperatures (T_{flow}) are also sharp and particularly high when tetra-amide segments are used. This DMTA behaviour is typical for segmented block copolymers with monodisperse crystallisable amide segments [20,30]. Polymers with monodisperse diamide segments ($x_m=1$) have somewhat higher T_g's and flex temperatures than polymers with monodisperse tetra-amide segments ($x_m=2$). Probably, some of the non-crystallised diamide

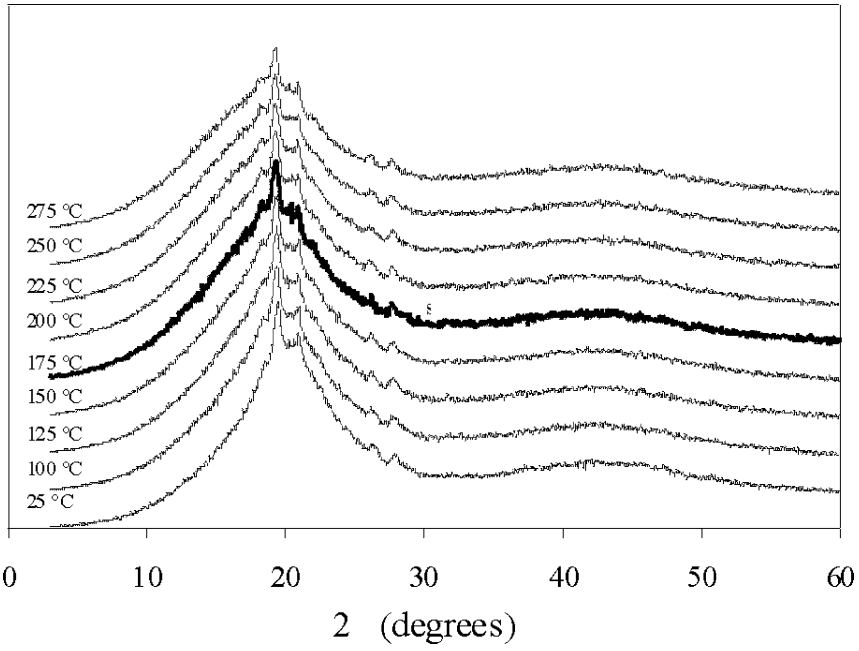

Fig. 7. WAXD pattern as function of temperature with random amide segments ($x_r=2$) ($T_{flow}=179$ °C).

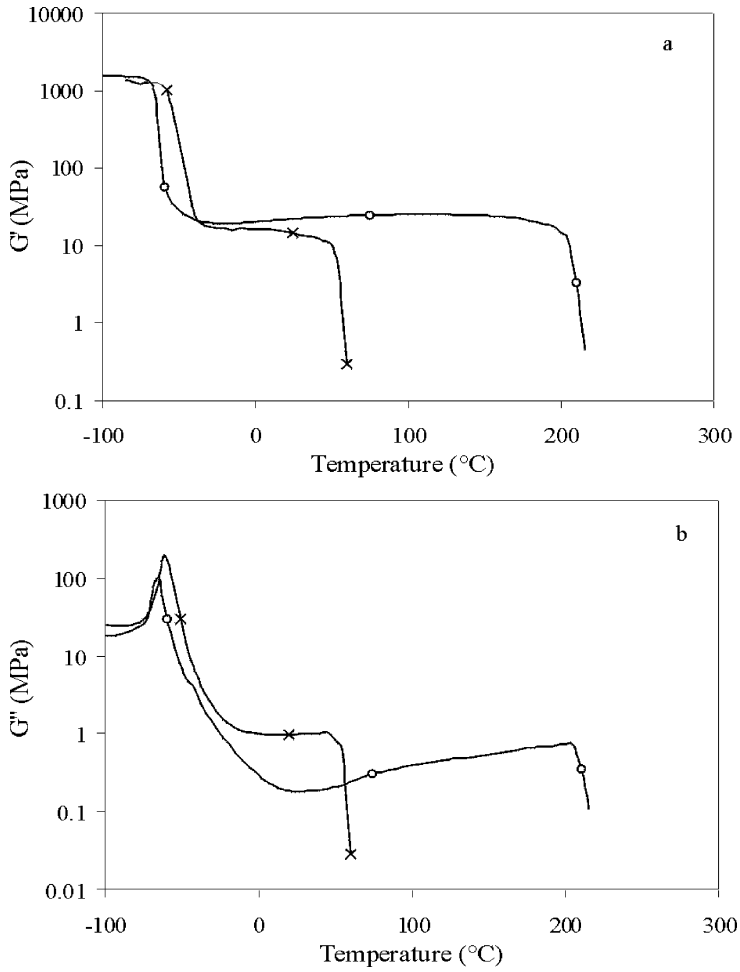

Fig. 8. Storage (G') (a) and loss modulus (G'') (b) as function of temperature of poly(propylene oxide) PEEA's with monodisperse amide segments. Amide segment length x_m: (×) 1 (11.2 wt%); (○) 2 (19.2 wt%).

segments remain dissolved in the PEO–PPO–PEO phase, thereby increasing the T_g of this phase. The flow temperatures of polymers with diamide segments are lower than with tetra-amide segments, as were the melting temperatures as measured by DSC (Table 2). On the other hand, the storage moduli of polymers with either diamide or tetra-amide segments are at room temperature similar.

Block copolymers with random amide segments were studied by DMTA too (Table 1, Fig. 9). The T_g of the soft matrix phase is sharp, close to −60 °C and little dependant on segment length. This is an indication that the amount of dissolved amide in the PEO–PPO–PEO phase is low and does not change with segment length. The flex temperatures are low ($T_{flex} = -40$ °C) which is due to the use of amorphous PEO–PPO–PEO_{2300}.

The modulus in the plateau region decreases with temperature but this temperature effect is small. The reason for this is probably the early melting of small imperfect crystals. The modulus at room temperature is strongly dependent on the amide segment length (amide concentration). The flow transition is broad and increases with amide segment length. In the TEM picture for $x_r = 2$ (Fig. 3(c)) a liquid–liquid phase separated phase was observed with possibly a salami type morphology (Fig. 2(c)). The submicron spheres are large compared to the amide segment length consist of an amide continues phase with in it PPO nano spheres. A separate transition for this phase was, however, not observed. Possibly the glass transition and melting temperature of the amide segments lay close to each other, giving a broad flow transition.

The difference of the monodisperse segments over the random length segments is that the T_g and particular the T_{flex} are somewhat lower, suggesting a better phase separation (Table 1, Figs. 8 and 9). Also the modulus at room temperature is appreciable higher and the modulus less temperature dependant, indicating a higher amide crystallinity and a neater lamellar structure. The melting temperature with monodisperse amide segments are more dependant on the amide length and for $x_m = 2$ higher than for $x_r = 2$ and melting transitions are sharper. With monodisperse amide segments the crystallites are more effective in increasing the modulus and melt at a well-defined temperature.

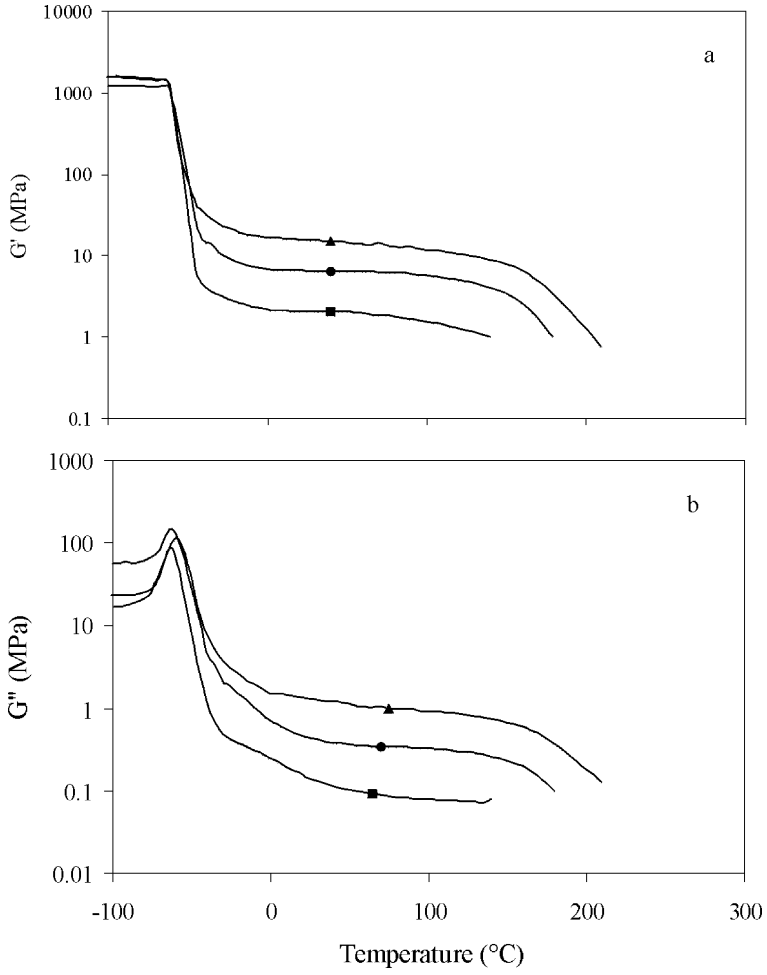

Fig. 9. Storage (G') (a) and loss modulus (G'') (b) as function of temperature of poly(propylene oxide) PEEA's random crystallisable amide segments. Random amide segment length x_r: (■) 1 (11.7 wt%); (●) 2 (19.6 wt%); (▲) 3 (29.1 wt%).

With increasing amide segment length (x) the (log) storage modulus (G' (25 °C)) increases (Fig. 10). With monodisperse amide segments, the modulus is 4–10 times higher than with random amide segments. The high modulus of PEEA's with monodisperse amide segments is probably due to the high crystallinity of the amide segments [20,30] and the strong reinforcing effect of the crystalline ribbons with a high aspect ratio (400–1000) (Fig. 3(a)). Monodisperse amide segments are, therefore, very effective in reinforcing the ether phase.

With random amide segments, both crystalline ribbons and spherical structures are present (Fig. 3(d)). The crystalline ribbons reinforce the ether phase, however, their aspect ratio is now 50–100. The amide segments in the spherical domains are little effective in increasing the modulus. With random amide segment length the reinforcing effect is, therefore, mainly due to the amide segments in the crystalline ribbons. The lower modulus observed for random amide segments is, thus, due to the partial crystallization and the low aspect ratio of the crystallites.

3.7. Compression set

The elasticity of the PEEA's was studied by means of compression set (CS) experiments. The compression set values are plotted as function of the amide segment length of PEEA's with either monodisperse or random amide segments (Table 1, Fig. 11).

With monodisperse amide segments, the compression set decreases strongly with increasing the amide segment length and the CS value for $x_m = 2$ is only 11%. Tetra-amide segments give thicker crystallites and thicker crystallites are expected to be more resistant to deformation than thinner crystals. The unusual thing is that polymers with monodisperse tetra-amide segments have compared monodisperse diamide segments a lower compression sets and at the same time a higher modulus. This is opposite to the general observed trend that as the modulus increases the set values also increases [20,22,31].

With random amide segments the CS-values increase with increasing segment length and the set values are not particular low. This increase in CS-values with increasing

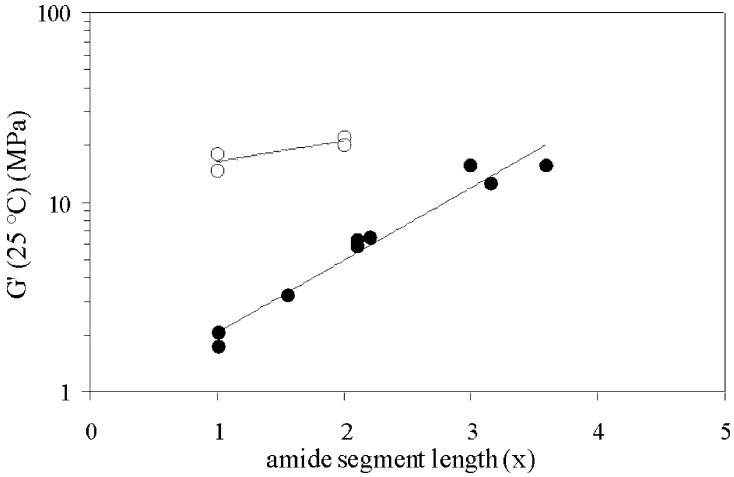

Fig. 10. The storage modulus (G' at 25 °C) of PEEA's as function of the amide segment length x. (○) monodisperse amide segment length; (●) random amide segment length.

amide length and, thus, increasing modulus is the trend, which is frequently observed [20,22,31]. The cause for this behaviour in compression set must be sought in the morphology of these materials. With random amide segments both short and long segments are present and the short diamide segments are less resistant to deformation. In addition, with increasing the average amide segment length liquid–liquid demixing is favoured and the liquid–liquid demixed domains are less resistant to deformation than the crystalline hard domains [22].

For the morphology with non-crystallisable liquid–liquid demixed domains the CS values decrease with amide segment length, however, the CS values are up to $x=3$ still very high (>50%) [22]. In going form a fully crystallized to a completely liquid–liquid phase separated system with $x=2$ the CS increases from 11 to 50%. Thus, increasing the liquid–liquid phase content increases the CS, despite the effect of the longer amide segment. The compression set of segmented block copolymers is apparently sensitive to the thickness of the crystallites and the presence of liquid–liquid demixed domains. If crystallisable monodisperse tetra-amide segments are employed both thin crystallites ($x=1$) and liquid–liquid demixed domains are absent. This results in low CS-values in combination with a relatively high modulus, which is a very interesting synergy of properties.

3.8. Recovery

In a standard ASTM compression set experiment, the compression set is measured after 30 min (1800 s) after the sample is unloaded. As the recovery of polymers is a time dependant (viscoelastic) process the recovery of several copolymers was monitored as function of time over a period of several weeks ($30–1\times10^6$ s) (Fig. 12).

The CS-values after 30 s (the first measurement) differed greatly with the type of amide segment. The polymer with $x_m=2$ had after 30 s already a low value while $x_m=1$ and

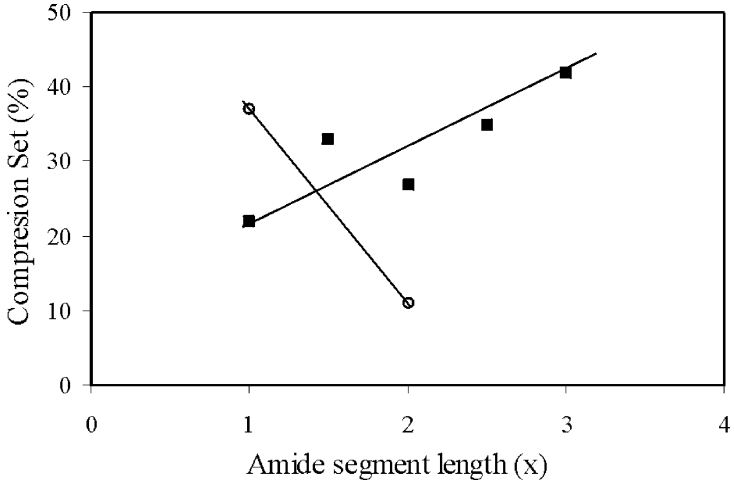

Fig. 11. Compression set at 20 °C as function of amide segment length: (○) Monodisperse amide segments; (■) random amide segments.

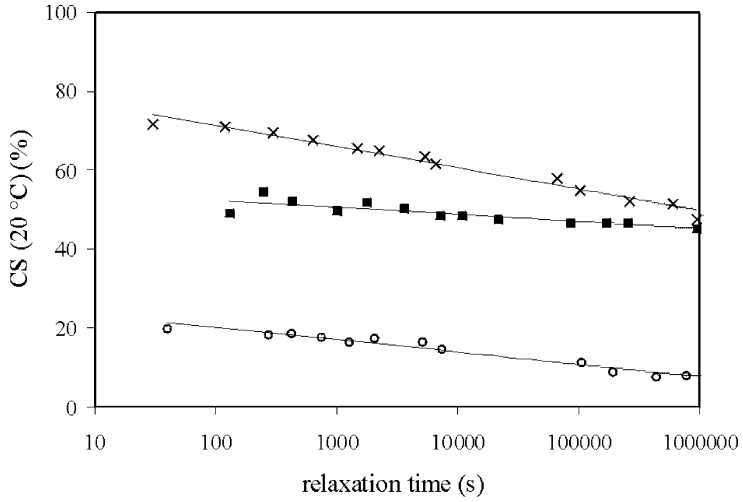

Fig. 12. Compression set at 20 °C as function of the relaxation time for different PEEA copolymers: (×) $x_m=1$; (○) $x_m=2$; (■) $x_r=3$ (note: The polymer with $x_m=1$ monodisperse is a different sample than described in Table 1).

$x_r=3$ had high values. With time (10^6 s) these values decreased a 10% in the CS-value. The decrease was faster for the materials containing the monodisperse amide segments. The initial (elastic) recovery is for these materials more important than the viscoelastic recovery, although for $x_m=2$ the CS-values more than halved during this recovery. Chemically cross linked PPO has a very high elastic recovery, a CS of 5% and fully recovered after 10^5 s [32]. The elastic recovery in the PEEA copolymers is, thus, due to the relaxation of the PPO segments. This viscoelastic recovery may be associated with a rearrangement in the crystalline amide phase [19,33]. The remaining deformation is probably a plastic deformation of the crystalline phase. This plastic deformation is much less for $x_m=2$ than for the other two materials. The rate viscoelastic recovery seems to be independent of the amount of plastic deformation.

3.9. Tensile set

The elastic behaviour in tensile is studied by tensile set (TS) in a cyclic tensile test with a step wise increasing strain and the increment of remaining strain, as function of the applied strain step is determined. The TS-values increase with strain and level off after approximately 20% strain (Fig. 13). Probably at 20% strain, macroscopic yielding of the amide phase starts. At higher strains the TS-values are constant (like for $x_r=1$) than necking in the sample is taking place. The TS-values for $x_m=2$ gradual increase with strain and this is particular so at higher strains. This effect is typical for a strain hardening material.

When the TS for $x_m=2$ is compared with $x_m=1$, the TS-values are lower and also yielding a starts at higher strains. The longer tetra-amide segments deform less easily.

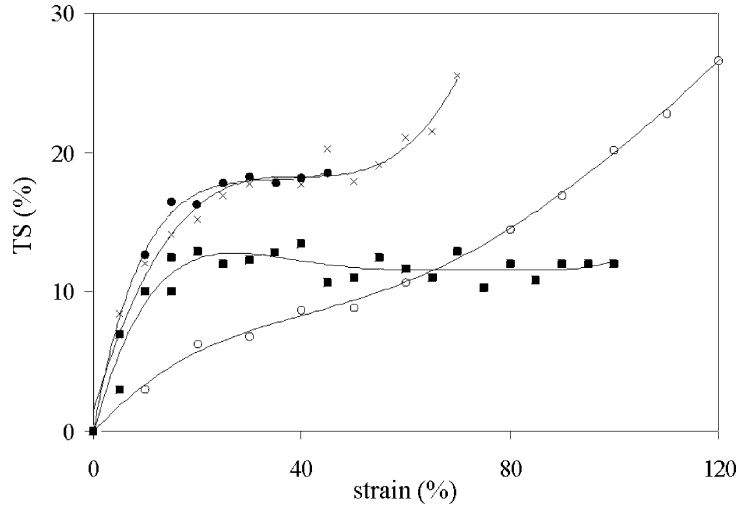

Fig. 13. The tensile set (TS) as function of strain: (×) $x_m=1$; (○) $x_m=2$; (■) $x_r=1$; (●) $x_r=2$.

If the $x_r=1$ and $x_r=2$ are compared than it is clear that the $x_r=1$ has lower TS-values. With $x_r=2$ the crystallites are on average thicker but at the same time the liquid–liquid demixing is stronger. It seems as if the liquid–liquid demixed phase increases the TS-values. If the TS for $x_m=2$ is compared with $x_r=2$, the TS-values are lower and also yielding starts at higher strains. The observed behaviour in tensile set is consistent with the trends observed in the compression set of these block copolymers.

4. Conclusions

Poly(propylene oxide) based polyether(ester–amide)s (PEEA) with monodisperse or random length amide crystallisable segments were synthesized and studied. With monodisperse segments, transparent elastic materials were obtained. The amide segments had crystallised in nano-ribbons with a high aspect ratio (400–1000). These polymers have low glass transition temperatures and a nearly temperature independent modulus in the rubber region. With increasing the amide segment length the melting temperature increases, the modulus increases and the compression set and tensile set values decreases.

With random length amide segments melt phasing was observed during polymerization and opaque elastic materials were obtained. Due to melt phasing during synthesis, the inherent viscosities were relatively low. The morphology is now complex and consist of crystalline ribbons with an aspect ratio of 50–100 and large spherical domains (>1 μm). These copolymers have too a low T_g and a fairly temperature independent rubber plateau. With increasing random amide segment length, the melting temperatures increase, the modulus increases but the elastic properties decreases. However, the modulus, melting temperatures and elastic properties are lower than for the x_m materials. It seems that if the liquid–liquid demixed phase content increases the CS and TS values increases. Thus, having only crystalline structures is an advantage for obtaining a higher modulus and a more elastic behaviour.

With monodisperse tetra-amide segments, the block copolymer possesses excellent elasticity in combination with surprisingly high modulus. The observed conclusions, regarding the structure-property relations for the PEEA copolymers, are expected to apply to similar semi-crystalline segmented block copolymers such as segmented polyurethanes (e.g. PEUU's).

Acknowledgements

This research was financed by the Dutch Polymer Institute (DPI, The Netherlands), project number 137. The authors would like to thank Mr H. Nefzger (Bayer AG, Germany) for supplying the Acclaim™ Polyols. Mr Rico Keim and Mr Mark Smithers (MESA+institute, the Netherlands) are acknowledged for their help and expertise with the TEM-experiments.

References

[1] Holden G, Legge NR, Schroeder HE, editors. Thermoplastic elastomers: A comprehensive review. 1st ed. Munich: Hanser Publishers; 1987.
[2] Leibler L. Macromolecules 1980;13:1602.
[3] Elwell MJA, Ryan AJ, Stanford JL. In: Macosko CW, editor. RIM: Fundamentals in reaction injection molding. Munich: Carl Hanser Verlag; 1988 [chapter 9].
[4] Broos R, Herrington RM, Casati FM. Cell Polym 2000;19:169.
[5] Armistead JP, Wilkes GL. J Appl Polym Sci 1988;35:601.
[6] Elwell MJA, Ryan AJ, Gruenbauer HJM, Van Lieshout HC, Lidy W. Plast Rubber Compos Process Appl 1995;23.
[7] Elwell MJA, Ryan AJ, Gruenbauer HJM, Van Lieshout HC. Macromolecules 1996;26:2960.
[8] Kaushiva BD, Wilkes GL. Polymer 2000;41:6981.
[9] Kaushiva BD, Wilkes GL. Polymer 2000;41:6987.
[10] Li Y, Desper R, Chu B. Macromolecules 1992;25:7365.
[11] Koberstein JT, Russel TP. Macromolecules 1986;19:714.
[12] Tocha E, Janik H, Vancso GJ. J Macromol Sci, Phys 2002;B41:1291.
[13] Adams RK, Hoeschele GK. In: Holden G, Legge NR, Schroeder HE, editors. Thermoplastic elastomers: A comprehensive review. 1st ed. Munich: Hanser Publishers; 1987 [chapter 8].
[14] Harrell LL. Macromolecules 1969;2:607.
[15] Ng HN, Allegreza AE, Cooper SL. Polymer 1973;14:255.
[16] Eisenbach CD, Baumgartner M, Gunter G. In: Lal J, Mark JE, editors. Advances in elastomer and rubber elasticity. NY, USA: Plenum Press; 1985.
[17] Versteegen RM. Well-defined thermoplastic elastomers: Reversible networks based on hydrogen bonding, PhD Thesis. The Netherlands: University of Eindhoven; 2003.
[18] McLean RW, Sauer BB. J Polym Sci, Part B 1999;37:859.
[19] Sauer BB, Gaymans RJ, Niesten MCEJ. J Polym Sci, Part B 2004;42:1783.
[20] Krijgsman J, Husken D, Gaymans RJ. Polymer 2003;44:7573.
[21] Silver FM, Dobinson F. J Polym Sci, Part A 1977;15:2535.
[22] Van der Schuur JM, Van der Heide EE, Feijen J, Gaymans RJ. Polymer 2005;46:3616.
[23] Van der Schuur JM, Feijen J, Gaymans RJ. Polymer 2005;46:327.
[24] Lothmar J, Meyer K, Goldbach G. Makromol Chem 1988;189:2053.
[25] Sawyer LC, Grubb DT. Polymer microscopy. 2nd ed. London: Chapman&Hall; 1996.
[26] Kohan MI. In: Xenopoulos A, Clark ES, editors. Nylon plastic handbook. NY, USA: Hanser Publishers; 1995.
[27] Sperling LH. Introduction to physical polymer science. 3rd ed. NY, USA: Wiley; 2001.
[28] Flory P. Principles of polymer chemistry. 4th ed. Wisconsin: Cornell University Press; 1964 [chapter 13].
[29] Niesten MCEJ, Harkema S, Van der Heide E, Gaymans RJ. Polymer 2001;42:1131.
[30] Niesten MCEJ, Feijen J, Gaymans RJ. Polymer 2000;40:8487.
[31] Niesten MCEJ, Gaymans RJ. Polymer 2001;42:6199.
[32] Van der Schuur JM, van der Heide E, Feijen J, Gaymans RJ. Polymer 2004;45:2721.
[33] Sauer BB, McLean RW, Brill DJ, Londono DJ. J Polym Sci, Part B 1999;40:1727.